Journal of Fluids and Structures (1999) **13,** 381–397
Article No.: jfls.1999.0203 available online at http://www.idealibrary.com on IDEAL

THE DIFFRACTION OF SECOND-ORDER BICHROMATIC WAVES BY A SEMI-IMMERSED HORIZONTAL RECTANGULAR CYLINDER

W. Li and A. N. Williams

Department of Civil & Environmental Engineering, University of Houston Houston, TX 77204–4791, U.S.A.

(Received 11 February 1998 and in revised form 28 October 1998)

The diffraction of second-order bichromatic Stokes waves by a semi-immersed horizontal rectangular cylinder (prism) is investigated theoretically. The problem is assumed two-dimensional and the fluid domain is divided into three regions: upwave, beneath and downwave of the structure. Analytical expressions for the velocity potentials in each region at both first- and second-order are obtained by an eigenfunction expansion approach. The solutions in each fluid region are linked through matching conditions on the imaginary fluid interfaces between them. Semi-analytical expressions are derived for the sum-and difference-frequency hydrodynamic loads and the free-surface elevations upwave and downwave of the structure to second-order. Numerical results are presented which illustrate the influence of the different wave and structural parameters on these quantities at both first- and second-order.

1. INTRODUCTION

The two-dimensional problem of second-order wave interaction with a long submerged or semi-immersed cylinder of circular or rectangular section, has been the subject of several previous investigations in recent years. These studies have employed a variety of analytical and numerical techniques. Wu & Eatock Taylor (1990) calculated the second-order diffraction force on a submerged circular cylinder in water of finite depth, using a method analogous to the three-dimensional "assisting radiation potential" approach of Lighthill (1979) and Molin (1979). Miao & Liu (1986) and Vada (1987) used similar approaches for the infinite depth case. Wu (1991) calculated the second-order reflection and transmission coefficients due to wave diffraction by a submerged circular cylinder. Later, Wu (1993a) also studied the problem of second-order wave radiation by the same body. Isaacson & Cheung (1990, 1991), and Isaacson & Ng (1993), have developed second-order time-domain solutions for the two-dimensional scattering and radiation problems respectively.

There have also been several approximate second-order analyses carried out. Newman (1990) developed a simplified solution for the second-order vertical force on a horizontal rectangular cylinder, based upon a deep submergence approximation. Wu (1993b) considered the hydrodynamic forces on a deeply submerged circular cylinder undergoing large-amplitude motion using a linearized free-surface condition but the exact body boundary condition. Sulisz & Johansson (1992) presented an approximate solution for the second-order wave loading on a semi-immersed rectangular cylinder. Sulisz (1993) subsequently presented an exact second-order solution to this problem for monochromatic incident waves.

0889–9746/99/040381 + 17 $30.00

The present paper considers the diffraction of second-order bichromatic waves by a semi-immersed horizontal rectangular cylinder (prism), and may be considered as an extension of the monochromatic wave case considered by Sulisz (1993). However, in the present case, in addition to providing the hydrodynamic loads to second-order, the free-surface elevations upwave and downwave of the structure are also computed. The fluid domain is divided into three regions: upwave, beneath, and downwave of the structure. Analytical expressions for the velocity potentials in each region at both first and second order are obtained by an eigenfunction expansion approach. The solutions in each fluid region are linked through matching conditions on the imaginary fluid interfaces between them. Semi-analytical expressions are derived for the hydrodynamic loads and the free-surface elevations upwave and downwave of the structure to second-order for both the sum and difference frequencies. Numerical results are presented which illustrate the influence of the different wave and structural parameters on these quantities at both first and second-order.

2. THEORETICAL DEVELOPMENT

The geometry of the problem is shown in Figure 1. A long cylindrical body of rectangular section of width $2b$ and draft d is located in water of uniform depth h. The problem is idealized as two-dimensional, Cartesian coordinates (x, z) are employed with the z-axis directed vertically upwards from an origin at the still-water level at the centre of the body. This body is subjected to a train of nonlinear bichromatic Stokes waves propagating in the positive x-direction. Under the assumption of an ideal, homogeneous, incompressible fluid undergoing irrotational motion, the fluid motion may be described in terms of a velocity potential $\Phi(x, z, t)$ such that the fluid velocity vector $\mathbf{q} = \nabla\Phi$. The velocity potential and free-surface elevation $\Xi(x, t)$ are assumed expressible in Stokes series, namely

$$\Phi(x, z, t) = \varepsilon\Phi^{(1)}(x, z, t) + \varepsilon^2\Phi^{(2)}(x, z, t) + \cdots, \tag{1}$$

$$\Xi(x, t) = \varepsilon\Xi^{(1)}(x, t) + \varepsilon^2\Xi^{(2)}(x, t) + \cdots, \tag{2}$$

where ε is a small parameter related to the wave steepness (Sarpkaya & Isaacson 1981).

By utilizing the series expansions in equations (1) and (2) and expanding the free-surface boundary conditions as Taylor series about the still-water level, the full, nonlinear wave–structure interaction problem may be replaced by a sequence of linear problems, one

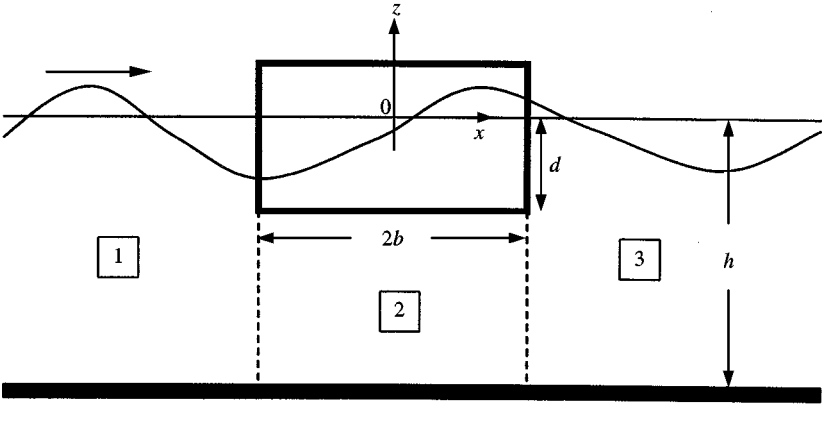

Figure 1. Definition sketch.

at each order of ε. In the present context, it is the $\mathcal{O}[\varepsilon]$ and $\mathcal{O}[\varepsilon^2]$ problems that are of interest.

If the incident wave system is taken to consist of a pair of waves of height H_i and frequency $\omega_j, j = 1, 2$, then the time dependency of the dynamic quantities can be separated explicitly as follows:

$$\Phi^{(1)}(x, z, t) = \mathscr{R}e \sum_{j=1}^{2} \phi_j^{(1)}(x, z) e^{-i\omega_j t}, \tag{3}$$

$$\Xi^{(1)}(x, t) = \mathscr{R}e \sum_{j=1}^{2} \eta_j^{(1)}(x) e^{-i\omega_j t}, \tag{4}$$

$$\Phi^{(2)}(x, z, t) = \mathscr{R}e \sum_{j=1}^{2} \sum_{k=1}^{2} [\phi_{jk}^{+}(x, z) e^{-i(\omega_j + \omega_k)t} + \phi_{jk}^{-}(x, z) e^{-i(\omega_j - \omega_k)t}] + B^{(2)} t, \tag{5}$$

$$\Xi^{(2)}(x, t) = \mathscr{R}e \sum_{j=1}^{2} \sum_{k=1}^{2} [\eta_{jk}^{+}(x) e^{-i(\omega_j + \omega_k)t} + \eta_{jk}^{-}(x) e^{-i(\omega_j - \omega_k)t}] + \frac{B^{(2)}}{g}, \tag{6}$$

where $\mathscr{R}e$ denotes the real part of a complex quantity, and $B^{(2)}$ is a constant (Stoker 1957).

The first-order, $\mathcal{O}[\varepsilon]$, problem may then be written as

$$\nabla^2 \phi_j^{(1)} = 0 \qquad \text{in the fluid domain,} \tag{7}$$

$$\frac{\partial \phi_j^{(1)}}{\partial z} = 0 \qquad \text{on } z = -h, \tag{8}$$

$$-\omega_j^2 \phi_j^{(1)} + g \frac{\partial \phi_j^{(1)}}{\partial z} = 0 \qquad \text{on } z = 0 \text{ for } |x| \geq b, \tag{9}$$

$$\frac{\partial \phi_j^{(1)}}{\partial n} = 0 \qquad \text{on the body surface.} \tag{10}$$

The surface elevation may be obtained from the potential via the linearized dynamic free-surface boundary condition,

$$\eta_j^{(1)} = \frac{i\omega_j}{g} \phi_j^{(1)} \quad \text{on } z = 0 \quad \text{for } |x| \geq b. \tag{11}$$

Finally, radiation conditions are required to ensure the correct asymptotic behaviour of the diffracted or scattered waves,

$$\lim_{x \to \infty} \left\{ \frac{\partial \phi_j^{(1)}}{\partial x} - i\gamma_{j0} \phi_j^{(1)} \right\} = 0, \tag{12}$$

$$\lim_{x \to -\infty} \left\{ \frac{\partial (\phi_j^{(1)} - \psi_{Ij}^{(1)})}{\partial x} + i\gamma_{j0} (\phi_j^{(1)} - \psi_{Ij}^{(1)}) \right\} = 0, \tag{13}$$

where $\psi_{Ij}^{(1)}$ is the complex spatial component of the incident potential,

$$\psi_{Ij}^{(1)} = -\frac{igH_j}{2\omega_j} e^{i\gamma_{j0} t} \frac{\cosh[\gamma_{j0}(z + h)]}{\cosh(\gamma_{j0} h)}, \tag{14}$$

in which γ_{j0} satisfies the linear dispersion relation for wave j, $\omega_j^2 = g\gamma_{j0} \tanh(\gamma_{j0} h)$.

The fluid domain is divided into three regions: region 1 for $x \leq -b,\ -h \leq z \leq 0$; region 2 for $-b \leq x \leq b,\ -h \leq z \leq -d$; and, region 3 for $x \geq b,\ -h \leq z \leq 0$. The potentials in each region are denoted by $\phi_{jn}^{(1)}$ for $n = 1, 2, 3$. The solutions in the three regions are related through continuity of pressure and velocity at the imaginary fluid interfaces between them, that is

$$\phi_{j1}^{(1)} = \phi_{j2}^{(1)}, \quad \frac{\partial \phi_{j1}^{(1)}}{\partial x} = \frac{\partial \phi_{j2}^{(1)}}{\partial x} \quad \text{on } x = -b,\ -h \leq z \leq -d, \tag{15}$$

$$\phi_{j3}^{(1)} = \phi_{j2}^{(1)}, \quad \frac{\partial \phi_{j3}^{(1)}}{\partial x} = \frac{\partial \phi_{j2}^{(1)}}{\partial x} \quad \text{on } x = b,\ -h \leq z \leq -d. \tag{16}$$

A suitable form for the velocity potential in region 1 which satisfies equations (7)–(9) and (13) is

$$\phi_{j1}^{(1)} = -\frac{\mathrm{i}g}{2\omega_j}\left\{H_j \mathrm{e}^{-k_{j0}(x+b)}\frac{\cos[k_{j0}(z+h)]}{\cos(k_{j0}h)} + \sum_{m=0}^{\infty} A_{jm}\mathrm{e}^{k_{jm}(x+b)}\frac{\cos[k_{jm}(z+h)]}{\cos(k_{jm}h)}\right\}, \tag{17}$$

in which $k_{j0} = -\mathrm{i}\gamma_{j0}$ and the $k_{jm}, m \geq 0$, are the positive real roots of $\omega_j^2 = -gk_{jm}\tan(k_{jm}h)$. The velocity potential in region 2, which satisfies equations (7), (8) and (10), may be written as

$$\phi_{j2}^{(1)} = -\frac{\mathrm{i}g}{\omega_j}\left\{(C_{j0}\frac{x}{b} + D_{j0}) + \sum_{m=1}^{\infty}\left[C_{jm}\frac{\cosh(\mu_m x)}{\cosh(\mu_m b)} + D_{jm}\frac{\sinh(\mu_m x)}{\sinh(\mu_m b)}\right]\cos[\mu_m(z+h)]\right\}, \tag{18}$$

where $\mu_m = m\pi/(h-d)$, for $m \geq 1$. The corresponding solution for region 3, satisfying equations (7), (8), (9) and (12), is

$$\phi_{j3}^{(1)} = -\frac{\mathrm{i}g}{\omega_j}\sum_{m=0}^{\infty} B_{jm}\mathrm{e}^{-k_{jm}(x-b)}\frac{\cos[k_{jm}(z+h)]}{\cos(k_{jm}h)}. \tag{19}$$

The potential coefficients A_{jm}, B_{jm} C_{jm}, and D_{jm}, for $m = 0, 1, 2, \ldots, j = 1, 2$, are determined by applying the matching conditions and structural boundary conditions at the interfaces between each region and utilizing the orthogonality of the vertical eigenfunctions over their region of validity. By manipulating these expressions, a system of equations may be obtained for each of the potential coefficients in turn. Truncating the infinite series that appear in these equations after a finite number of terms allows the equations for the potential coefficients to be solved by standard matrix techniques. Once the velocity potentials have been determined, the free-surface elevations upwave and downwave of the structure may be calculated from equation (11).

The second-order, $\mathcal{O}[\varepsilon^2]$, problem may then be written as

$$\nabla^2\phi_{jk}^{\pm} = 0 \qquad \text{in the fluid domain,} \tag{20}$$

$$\frac{\partial \phi_k^{\pm}}{\partial z} = 0 \qquad \text{on } z = -h, \tag{21}$$

$$\frac{\partial \phi_{jk}^{\pm}}{\partial n} = 0 \qquad \text{on the body surface.} \tag{22}$$

The free-surface condition at second-order is more involved than that at first-order. Therefore, it is convenient to first define the second-order potential components in each of the three fluid regions as $\phi_{jk}^{m\pm}$ for $m = 1, 2, 3$. Then the free-surface boundary conditions at second-order in regions 1 (upwave) and 3 (downwave) of the structure may be written as

$$g\frac{\partial \phi_{jk}^{1\pm}}{\partial z} - \phi_{jk}^{1\pm}(\omega_j \pm \omega_k)^2 = Q_{jk}^{1\pm} \quad \text{on } z = 0 \quad \text{for } x \leq -b, \tag{23}$$

$$g\frac{\partial \phi_{k}^{3\pm}}{\partial z} - \phi_{jk}^{3\pm}(\omega_j \pm \omega_k)^2 = Q_{jk}^{3\pm} \quad \text{on } z = 0 \quad \text{for } x \geq b, \tag{24}$$

in which

$$Q_{jk}^{1+} = \frac{2\omega_j^2\omega_k^3 + \omega_j\omega_k^4}{2g^2}\,\mathrm{i}\phi_{j1}^{(1)}\phi_{k1}^{(1)} + \mathrm{i}\omega_k\frac{\partial \phi_{j1}^{(1)}}{\partial x}\frac{\partial \phi_{k1}^{(1)}}{\partial x} + \frac{\mathrm{i}\omega_j}{2}\phi_{j1}^{(1)}\frac{\partial^2 \phi_{k1}^{(1)}}{\partial x^2}, \tag{25a}$$

$$Q_{jk}^{1-} = \frac{\omega_j\omega_k^4 - 2\omega_j^2\omega_k^3}{2g^2}\,\mathrm{i}\phi_{j1}^{(1)}\bar{\phi}_{k1}^{(1)} - \mathrm{i}\omega_k\frac{\partial \phi_{j1}^{(1)}}{\partial x}\frac{\partial \bar{\phi}_{k1}^{(1)}}{\partial x} + \frac{\mathrm{i}\omega_j}{2}\phi_{j1}^{(1)}\frac{\partial^2 \bar{\phi}_{k1}^{(1)}}{\partial x^2}, \tag{25b}$$

$$Q_{jk}^{3+} = \frac{2\omega_j^2\omega_k^3 + \omega_j\omega_k^4}{2g^2}\,\mathrm{i}\phi_{j3}^{(1)}\phi_{k3}^{(1)} + \mathrm{i}\omega_k\frac{\partial \phi_{j3}^{(1)}}{\partial x}\frac{\partial \phi_{k3}^{(1)}}{\partial x} + \frac{\mathrm{i}\omega_j}{2}\phi_{j3}^{(1)}\frac{\partial^2 \phi_{k3}^{(1)}}{\partial x^2}, \tag{26a}$$

$$Q_{jk}^{3-} = \frac{\omega_j\omega_k^4 - 2\omega_j^2\omega_k^3}{2g^2}\,\mathrm{i}\phi_{j3}^{(1)}\bar{\phi}_{k3}^{(1)} - \mathrm{i}\omega_k\frac{\partial \phi_{j3}^{(1)}}{\partial x}\frac{\partial \bar{\phi}_{k3}^{(1)}}{\partial x} + \frac{\mathrm{i}\omega_j}{2}\phi_{j3}^{(1)}\frac{\partial^2 \bar{\phi}_{k3}^{(1)}}{\partial x^2}, \tag{26b}$$

In equations (25b) and (26b) the overbars denote complex conjugates. The second-order surface elevation components may be obtained from the corresponding potentials via the dynamic free-surface boundary condition to yield

$$\eta_{jk}^{+} = \frac{\mathrm{i}(\omega_j + \omega_k)}{g}\phi_{jk}^{+} - \frac{1}{4g}\frac{\partial \phi_j^{(1)}}{\partial x}\frac{\partial \phi_k^{(1)}}{\partial x} - \frac{\omega_j^2\omega_k^2 + 2\omega_j\omega_k^3}{4g^3}\phi_j^{(1)}\phi_k^{(1)} \quad \text{on } z = 0 \text{ for } |x| \geq b, \tag{27a}$$

$$\eta_{jk}^{-} = \frac{\mathrm{i}(\omega_j - \omega_k)}{g}\phi_{jk}^{-} - \frac{1}{4g}\frac{\partial \phi_j^{(1)}}{\partial x}\frac{\partial \bar{\phi}_k^{(1)}}{\partial x} - \frac{\omega_j^2\omega_k^2 - 2\omega_j\omega_k^3}{4g^3}\bar{\phi}_j^{(1)}\phi_k^{(1)} \quad \text{on } z = 0 \text{ for } |x| \geq b. \tag{27b}$$

Finally, radiation conditions are required to ensure the correct asymptotic behaviour of the second-order diffracted or scattered waves. At large distances from the structure, the scattered wave field will consist of free and forced waves. The free waves satisfy a homogeneous free-surface condition and a radiation condition similar to that at first order but with corresponding changes of wave number, namely

$$\lim_{x \to \pm\infty}\left\{\frac{\partial \Theta_{jk}^{\pm}}{\partial x} \mp \mathrm{i}\gamma_{jk0}^{\pm}\Theta_{jk}^{\pm}\right\} = 0, \tag{28}$$

in which $\Theta_{jk}^{\pm}$ represents the second-order sum- and difference-frequency free wave potential, whose propagating free wave numbers $\gamma_{jk0}^{\pm}$ satisfy the dispersion relation $(\omega_j \pm \omega_k)^2 = g\gamma_{jk0}^{\pm}\tanh(\gamma_{jk0}^{\pm}h)$. The correct asymptotic behaviour of the second-order forced wave field is determined from the asymptotic form of the second-order free-surface boundary condition.

Explicit forms for the second-order velocity potentials in regions 1–3 that satisfy the appropriate boundary conditions on the free-surface, sea-bed, and at infinity, are presented below:

$$\phi_{jk}^{1+} = T(-k_{k0}, -k_{j0}, \omega_k, \omega_j) H_j H_k \mathrm{e}^{-(k_{k0}+k_{j0})(x+b)} \frac{\cos[(k_{j0}+k_{k0})(z+h)]}{\cos(k_{j0}h)\cos(k_{k0}h)}$$
$$+ \sum_{m=0}^{\infty} T(-k_{k0}, k_{jm}, \omega_k, \omega_j) A_{jm} H_k \mathrm{e}^{(k_{jm}-k_{k0})(x+b)} \frac{\cos[(k_{jm}-k_{k0})(z+h)]}{\cos(k_{jm}h)\cos(k_{k0}h)}$$
$$+ \sum_{n=0}^{\infty} T(k_{kn}, -k_{j0}, \omega_k, \omega_j) H_j A_{kn} \mathrm{e}^{(k_{kn}+k_{j0})(x+b)} \frac{\cos[(k_{j0}-k_{kn})(z+h)]}{\cos(k_{j0}h)\cos(k_{kn}h)}$$
$$+ \sum_{m=0}^{\infty}\sum_{n=0}^{\infty} T(k_{kn}, k_{jm}, \omega_k, \omega_j) A_{jm} A_{kn} \mathrm{e}^{(k_{km}+k_{jn})(x+b)} \frac{\cos[(k_{jm}+k_{kn})(z+h)]}{\cos(k_{jm}h)\cos(k_{kn}h)}$$
$$+ \sum_{m=0}^{\infty} R_{jkm}^{+} \mathrm{e}^{\alpha_{jkm}^{+}(x+b)} \frac{\cos[\alpha_{jkm}^{+}(z+h)]}{\cos(\alpha_{jkm}^{+}h)}, \tag{29}$$

$$\phi_{jk}^{1-} = T(-\bar{k}_{k0}, -k_{j0}, -\omega_k, \omega_j) H_j \bar{H}_k \mathrm{e}^{-(\bar{k}_{k0}+k_{j0})(x+b)} \frac{\cos[(k_{j0}+\bar{k}_{k0})(z+h)]}{\cos(k_{j0}h)\cos(\bar{k}_{k0}h)}$$
$$+ \sum_{m=0}^{\infty} T(-\bar{k}_{k0}, k_{jm}, -\omega_k, \omega_j) A_{jm} \bar{H}_k \mathrm{e}^{(k_{jm}-\bar{k}_{k0})(x+b)} \frac{\cos[(k_{jm}-\bar{k}_{k0})(z+h)]}{\cos(k_{jm}h)\cos(\bar{k}_{k0}h)}$$
$$+ \sum_{n=0}^{\infty} T(\bar{k}_{kn}, -k_{j0}, -\omega_k, \omega_j) H_j \bar{A}_{kn} \mathrm{e}^{(\bar{k}_{kn}+k_{j0})(x+b)} \frac{\cos[(k_{j0}-\bar{k}_{kn})(z+h)]}{\cos(k_{j0}h)\cos(\bar{k}_{kn}h)}$$
$$+ \sum_{m=0}^{\infty}\sum_{n=0}^{\infty} T(\bar{k}_{kn}, k_{jm}, -\omega_k, \omega_j) A_{jm} \bar{A}_{kn} \mathrm{e}^{(\bar{k}_{km}+k_{jn})(x+b)} \frac{\cos[(k_{jm}+\bar{k}_{kn})(z+h)]}{\cos(k_{jm}h)\cos(\bar{k}_{kn}h)}$$
$$+ \sum_{m=0}^{\infty} R_{jkm}^{-} \mathrm{e}^{\alpha_{jkm}^{-}(x+b)} \frac{\cos[\alpha_{jkm}^{-}(z+h)]}{\cos(\alpha_{jkm}^{-}h)}, \tag{30}$$

$$\phi_{jk}^{2\pm} = C_{jk0}^{\pm} + D_{jk0}^{\pm} + \sum_{m=1}^{\infty} \left[C_{jkm}^{\pm} \frac{\cosh(\mu_m x)}{\sinh(\mu_m b)} + D_{jkm}^{\pm} \frac{\sinh(\mu_m x)}{\cosh(\mu_m b)} \right] \cos[\mu_m(z+h)], \tag{31}$$

$$\phi_{jk}^{3+} = \sum_{m=0}^{\infty}\sum_{n=0}^{\infty} T(k_{kn}, k_{jm}, \omega_k, \omega_j) B_{jm} B_{kn} \mathrm{e}^{-(k_{km}+k_{jn})(x+b)} \frac{\cos[(k_{jm}+k_{kn})(z+h)]}{\cos(k_{jm}h)\cos(k_{kn}h)}$$
$$+ \sum_{m=0}^{\infty} S_{jkm}^{+} \mathrm{e}^{-\alpha_{jkm}^{+}(x-b)} \frac{\cos[\alpha_{jkm}^{+}(z+h)]}{\cos(\alpha_{jkm}^{+}h)}, \tag{32}$$

$$\phi_{jk}^{3-} = \sum_{m=0}^{\infty}\sum_{n=0}^{\infty} T(\bar{k}_{kn}, k_{jm}, -\omega_k, \omega_j) B_{jm} \bar{B}_{kn} \mathrm{e}^{-(\bar{k}_{km}+k_{jn})(x-b)} \frac{\cos[(k_{jm}+\bar{k}_{kn})(z+h)]}{\cos(k_{jm}h)\cos(\bar{k}_{kn}h)}$$
$$+ \sum_{m=0}^{\infty} S_{jkm}^{-} \mathrm{e}^{-\alpha_{jkm}^{-}(x-b)} \frac{\cos[\alpha_{jkm}^{-}(z+h)]}{\cos(\alpha_{jkm}^{-}h)}, \tag{33}$$

in which the wave numbers $\alpha_{jkm}^{\pm} = \{-\mathrm{i}\gamma_{jk0}^{\pm}, \gamma_{jk1}^{\pm}, {}_{jk2}^{\pm}, \dots\}$, the $\gamma_{jkm}^{\pm}$ for $m = 1, 2, \dots$ are defined as the positive real roots of $(\omega_j \pm \omega_k)^2 + g\gamma_{jkm}\tan(\gamma_{jkm}h) = 0$. The last term in each of equations (29), (30), (32) and (33) represents the free-wave component of that potential. Also, in equations (29)–(33),

$$T(k_{kn}, k_{jm}, \omega_k, \omega_j) = \frac{-\mathrm{i}(2\omega_j^2\omega_k^3 + \omega_j\omega_k^4 + 2g^2k_{jm}k_{kn}\omega_k + g^2k_{kn}^2\omega_j)k_{jm}k_{kn}g^2}{2\omega_j\omega_k[(\omega_j + \omega_k)^2\omega_j^2\omega_k^2 + g^2(\omega_j k_{kn} - \omega_k k_{jm})^2]}. \tag{34}$$

When applying equation (34), if $m^2 + n^2 + (k-j)^2 = 0$, then $T(\,) = 0$ in the first and fourth terms of equation (30), and the first term of equation (32). The potential coefficients $R_{jkm}^{\pm}$ and $S_{jkm}^{\pm}$ are now found by applying the second-order matching conditions at the imaginary fluid interfaces between the three regions, and utilizing the orthogonality properties of the vertical eigenfunctions. The procedure is similar to that used to determine the first-order coefficients. The matching conditions at second-order are

$$\phi_{jk}^{1\pm} = \phi_{jk}^{2\pm}, \quad \frac{\partial\phi_{jk}^{1\pm}}{\partial x} = \frac{\partial\phi_{jk}^{2\pm}}{\partial x} \quad \text{on } x = -b, -h \le z \le -d, \tag{35}$$

$$\phi_{jk}^{3\pm} = \phi_{jk}^{2\pm}, \quad \frac{\partial\phi_{jk}^{3\pm}}{\partial x} = \frac{\partial\phi_{jk}^{2\pm}}{\partial x} \quad \text{on } x = b, -h \le z \le -d. \tag{36}$$

Once the second-order velocity potentials have been determined, the free-surface elevations at this order may be calculated from equation (27).

Other quantities of interest may now be determined; the hydrodynamic pressure to second-order is given by

$$P = -\rho gz - \varepsilon\rho\frac{\partial\Phi^{(1)}}{\partial t} - \varepsilon^2\rho\left\{\frac{1}{2}(\nabla\Phi^{(1)})^2 + \frac{\partial\Phi^{(2)}}{\partial t} - B^{(2)}\right\}. \tag{37}$$

If the hydrodynamic force and moment components are now expressed as perturbation series, in a similar manner to the velocity potential and free-surface elevation, namely

$$\mathbf{F}(t) = \varepsilon\mathbf{F}^{(1)}(t) + \varepsilon^2\mathbf{F}^{(2)}(t) + \cdots, \tag{38}$$

$$\mathbf{M}(t) = \varepsilon\mathbf{M}^{(1)}(t) + \varepsilon^2\mathbf{M}^{(2)}(t) + \cdots, \tag{39}$$

then the first- and second-order force and moment vectors may be written as

$$\mathbf{F}^{(1)}(t) = \mathscr{R}e\sum_{j=1}^{2}\mathbf{f}_j^{(1)}\mathrm{e}^{-\mathrm{i}\omega_j t}, \tag{40}$$

$$\mathbf{F}^{(2)}(t) = \mathscr{R}e\sum_{j=1}^{2}\sum_{k=1}^{2}[\mathbf{f}_{jk}^{+}\mathrm{e}^{-\mathrm{i}(\omega_j+\omega_k)t} + \mathbf{f}_{jk}^{-}\mathrm{e}^{-\mathrm{i}(\omega_j-\omega_k)t}], \tag{41}$$

$$\mathbf{M}^{(1)}(t) = \mathscr{R}e\sum_{j=1}^{2}\mathbf{m}_j^{(1)}\mathrm{e}^{-\mathrm{i}\omega_j t}, \tag{42}$$

$$\mathbf{M}^{(2)}(t) = \mathscr{R}e\sum_{j=1}^{2}\sum_{k=1}^{2}[\mathbf{m}_{jk}^{+}\mathrm{e}^{-\mathrm{i}(\omega_j+\omega_k)t} + \mathbf{m}_{jk}^{-}\mathrm{e}^{-\mathrm{i}(\omega_j-\omega_k)t}], \tag{43}$$

in which

$$\mathbf{f}_j^{(1)} = \int_{S_{BO}} \mathrm{i}\rho\omega_j \phi_j^{(1)} \mathbf{n}\, \mathrm{d}S, \tag{44}$$

$$\mathbf{f}_{jk}^{+} = \int_{S_{BO}} \left[\mathrm{i}\rho(\omega_j + \omega_k)\phi_{jk}^{+} - \frac{1}{4}\rho \nabla \phi_j^{(1)} \nabla \phi_k^{(1)} \right] \mathbf{n}\, \mathrm{d}S - \frac{1}{4g}\rho \int_{C_B} \omega_j \omega_k \phi_j^{(1)} \phi_k^{(1)} \mathbf{n}\, \mathrm{d}C, \tag{45}$$

$$\mathbf{f}_{jk}^{-} = \int_{S_{BO}} \left[\mathrm{i}\rho(\omega_j - \omega_k)\phi_{jk}^{-} - \frac{1}{4}\rho \nabla \phi_j^{(1)} \nabla \bar{\phi}_k^{(1)} \right] \mathbf{n}\, \mathrm{d}S + \frac{1}{4g}\rho \int_{C_B} \omega_j \omega_k \phi_j^{(1)} \bar{\phi}_k^{(1)} \mathbf{n}\, \mathrm{d}C, \tag{46}$$

$$\mathbf{m}_j^{(1)} = \int_{S_{BO}} \mathrm{i}\rho\omega_j \phi_j^{(1)} \mathbf{r} \times \mathbf{n}\, \mathrm{d}S, \tag{47}$$

$$\mathbf{m}_{jk}^{+} = \int_{S_{BO}} \left[\mathrm{i}\rho(\omega_j + \omega_k)\phi_{jk}^{+} - \frac{1}{4}\rho \nabla \phi_j^{(1)} \nabla \phi_k^{(1)} \right] \mathbf{r} \times \mathbf{n}\, \mathrm{d}S - \frac{1}{4g}\rho \int_{C_B} \omega_j \omega_k \phi_j^{(1)} \phi_k^{(1)} \mathbf{r} \times \mathbf{n}\, \mathrm{d}C, \tag{48}$$

$$\mathbf{m}_{jk}^{-} = \int_{S_{BO}} \left[\mathrm{i}\rho(\omega_j - \omega_k)\phi_{jk}^{-} - \frac{1}{4}\rho \nabla \phi_j^{(1)} \nabla \bar{\phi}_k^{(1)} \right] \mathbf{r} \times \mathbf{n}\, \mathrm{d}S + \frac{1}{4g}\rho \int_{C_B} \omega_j \omega_k \phi_j^{(1)} \bar{\phi}_k^{(1)} \mathbf{r} \times \mathbf{n}\, \mathrm{d}C. \tag{49}$$

In the above equations, S_{BO} indicates the equilibrium surface of the body up to the still-water level, and C_B indicates the waterline contour (waterline points).

Finally, the Bernoulli constant at second-order may be determined from the asymptotic behaviour of the wave field, and is given by

$$B^{(2)} = \frac{1}{8} \sum_{j=1}^{2} \left[|H_j|^2 + |A_{j0}|^2 + |B_{j0}|^2 \right] \frac{|k_{j0}|^2}{\omega_j^2 \cos(k_{j0}h)}. \tag{50}$$

3. NUMERICAL RESULTS AND DISCUSSION

Before considering the bichromatic wave case, a comparison was made with the monochromatic wave results of Sulisz (1993). Figure 2 presents a comparison of the second-order components of horizontal and vertical force, and the overturning moment about the point $x = b$, $z = -d$ obtained by the present computer program and the results of Sulisz. In the figures, the dimensionless wave number is $\gamma_{j0}h$, forces are non-dimensionalized by $\rho g(H_j/2)^2$ and moments by $\rho g h(H_j/2)^2$. The infinite series in the expressions for the first-order potentials in equations (17)–(19) were truncated after 30 terms, while the infinite series in the second-order potentials in equations (29), (31) and (32) were truncated after 60 terms. It can be seen that excellent agreement is exhibited over the entire frequency range of interest for each case considered. Therefore, the same truncations of the infinite potential series at first- and second-order were adopted in the bichromatic wave analysis.

The second-order hydrodynamic forces and moment, and surface elevations, for the case of bichromatic incident waves will now be presented. The numerical results are presented as dimensionless sum- or difference-frequency loads at a fixed sum or difference frequency, for varying difference or sum frequency, respectively. The forces are nondimensionalized by $\rho g(H_1^2 + H_2^2)/4$ and the moment by $\rho g d(H_1^2 + H_2^2)/4$. Figure 3 presents the variation of the dimensionless second-order, sum-frequency forces and moments for $(\omega_1 + \omega_2) = 4{\cdot}0$ rad/s, and $b/h = 1$, $d/h = 0{\cdot}4$ with difference frequency $(\omega_1 - \omega_2)$, also in rad/s. It can be seen that, in general, the sum-frequency terms, $(\omega_j + \omega_k)$, $j \neq k$, are largest at the largest difference frequencies, while the double-frequency terms, ω_i, are a maximum at zero difference

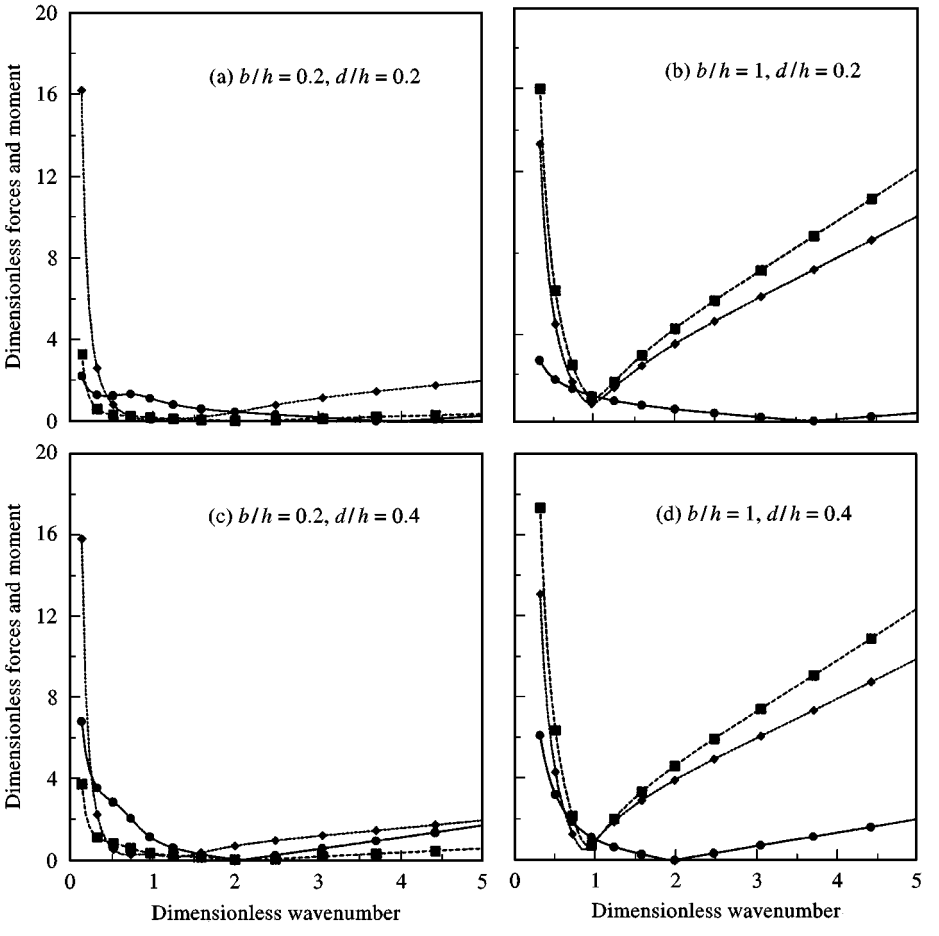

Figure 2. Comparison of second-order horizontal (—, ●) and vertical forces (- - - - -, ◆), and overturning moment (– – –, ■) computed by present approach (lines) and results of Sulisz (1993) (symbols)..

frequency. In Figure 4, it can be seen that the horizontal difference-frequency force components exhibit the same behaviour as their sum-frequency counterparts, while all components of the second-order vertical difference-frequency force are strongly concentrated about the zero difference frequency. This implies that the mean second-order vertical force is the dominant contribution to the low-frequency vertical loading. The moment in Figure 4 is clearly a combination of the horizontal and vertical force components.

Figures 5 and 6 present, respectively, the variation of the dimensionless second-order, sum- and difference-frequency forces and moments for $(\omega_1 - \omega_2) = 1{\cdot}0$ rad/s, and $b/h = 1$, $d/h = 0{\cdot}4$ with sum-frequency $(\omega_1 + \omega_2)$, also in rad/s. From Figure 5, it can be seen that, for all loading components, the sum-frequency loads, at frequencies $(\omega_j + \omega_k)$, $j \neq k$, are dominant, and are largest at the sum frequencies. In Figure 6, it can be seen that the difference-frequency loading, at frequencies $(\omega_j - \omega_k)$, $j \neq k$, again dominates the mean (zero difference-frequency) loading.

One advantage of pursuing a complete solution for the second-order potential, rather than just a solution for the second-order loads through an assisting radiation potential

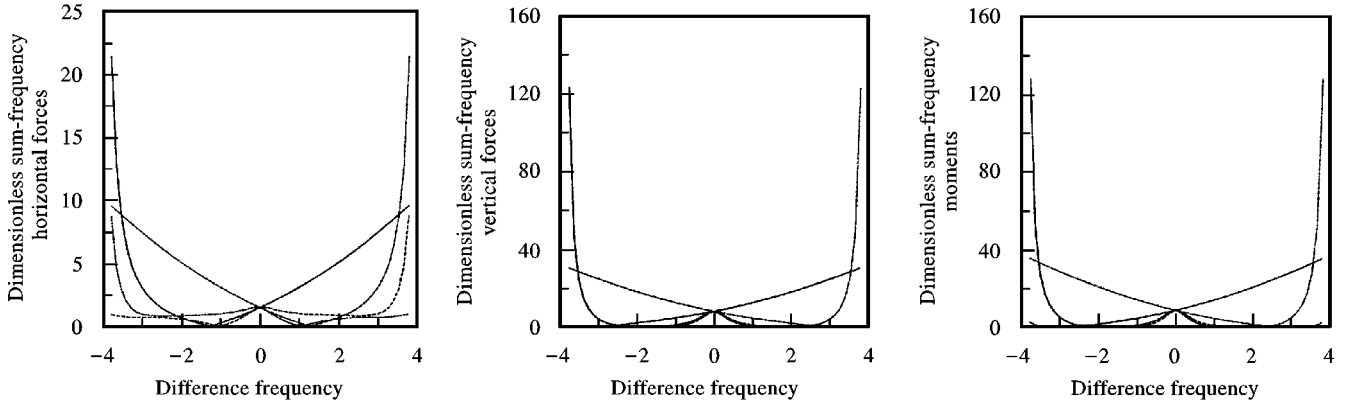

Figure 3. Dimensionless second-order, sum-frequency, horizontal and vertical forces, and moments about the point $x = b$, $z = -d$ for $(\omega_1 + \omega_2) = 4{\cdot}0$, and $b/h = 1$, $d/h = 0{\cdot}4$: ———, $2\omega_1$ components; –·–·–, $2\omega_2$ components; – – – – – – – –, $(\omega_1 + \omega_2)$ components; — — —, $(\omega_2 + \omega_1)$ components.

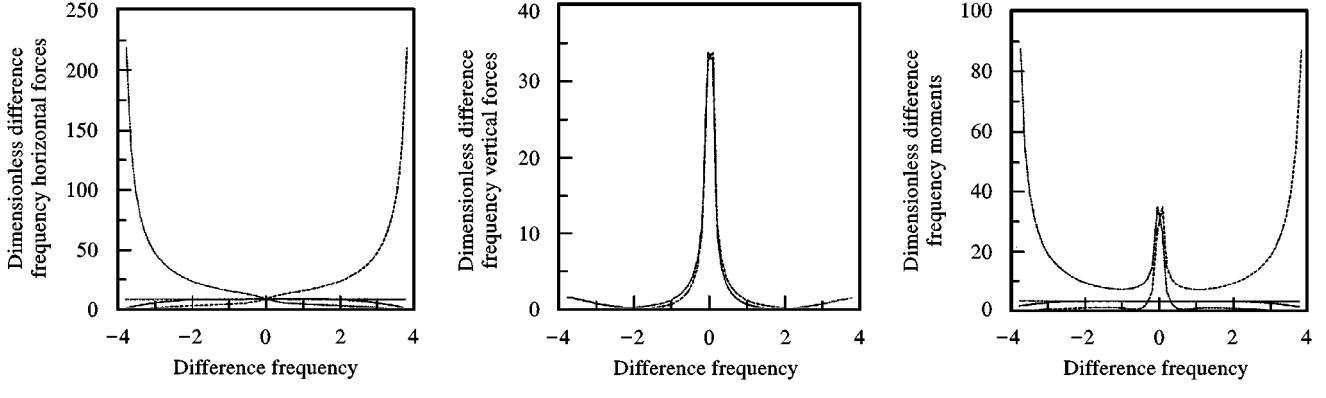

Figure 4. Dimensionless second-order, difference-frequency, horizontal and vertical forces, and moments about the point $x = b$, $z = -d$ for $(\omega_1 + \omega_2) = 4{\cdot}0$, and $b/h = 1$, $d/h = 0{\cdot}4$: ———, mean components arising from ω_1; –·–·–, mean components arising from ω_2; – – – – – – – –, $(\omega_1 - \omega_2)$ components; — — —, $(\omega_2 - \omega_1)$ components.

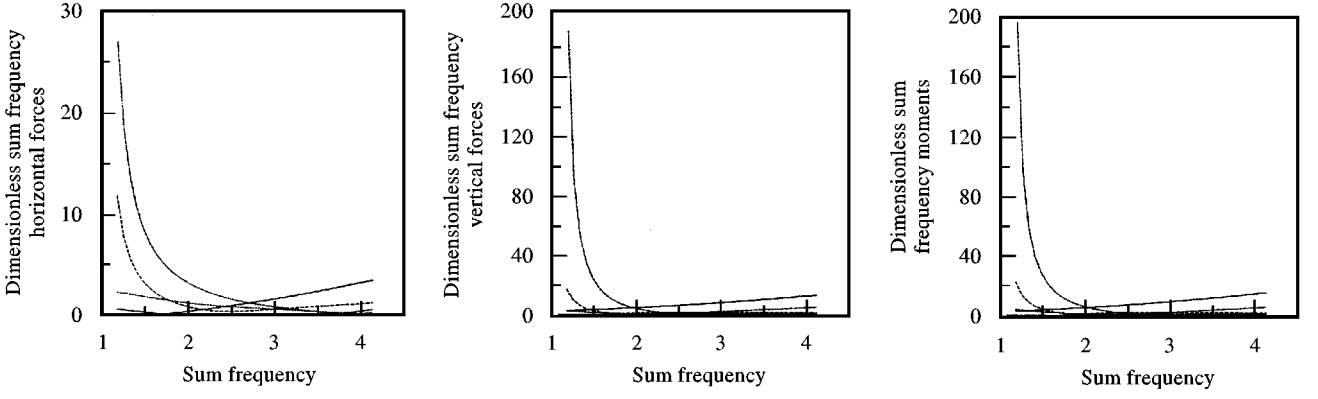

Figure 5. Dimensionless second-order, sum-frequency, horizontal and vertical forces, and moments about the point $x = b$, $z = -d$ for $(\omega_1 - \omega_2) = 1{\cdot}0$, and $b/h = 1$, $d/h = 0{\cdot}4$: ———, $2\omega_1$ components; –·–·–, $2\omega_2$ components; – – – – – – – –, $(\omega_1 + \omega_2)$ components; — — —, $(\omega_2 + \omega_1)$ components.

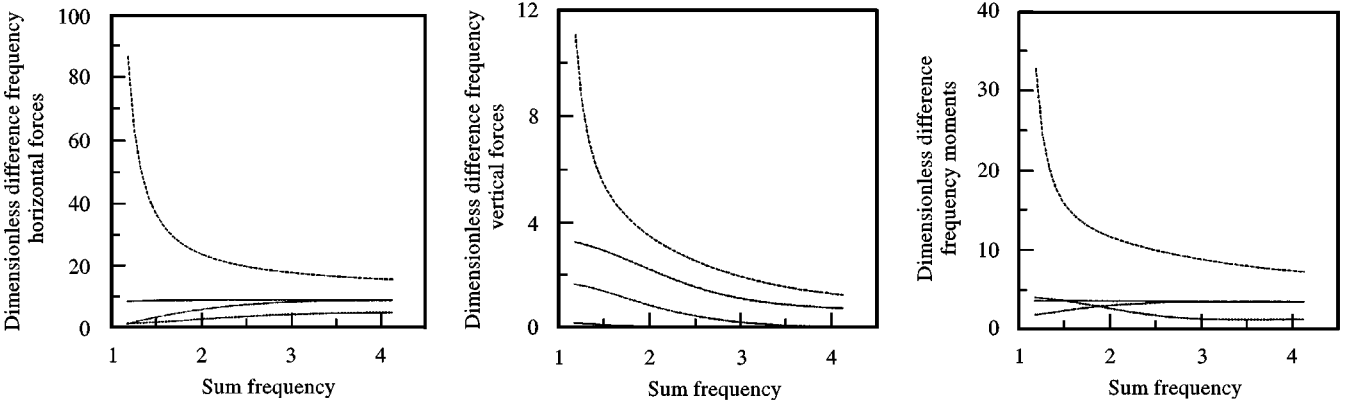

Figure 6. Dimensionless second-order, difference-frequency, horizontal and vertical forces, and moments about the point $x = b$, $z = -d$ for $(\omega_1 - \omega_2) = 1{\cdot}0$, and $b/h = 1$, $d/h = 0{\cdot}4$: ———, mean components arising from ω_1; –·–·–, mean components arising from ω_2; – – – – – – – –, $(\omega_1 - \omega_2)$ components; — — —, $(\omega_2 - \omega_1)$ components.

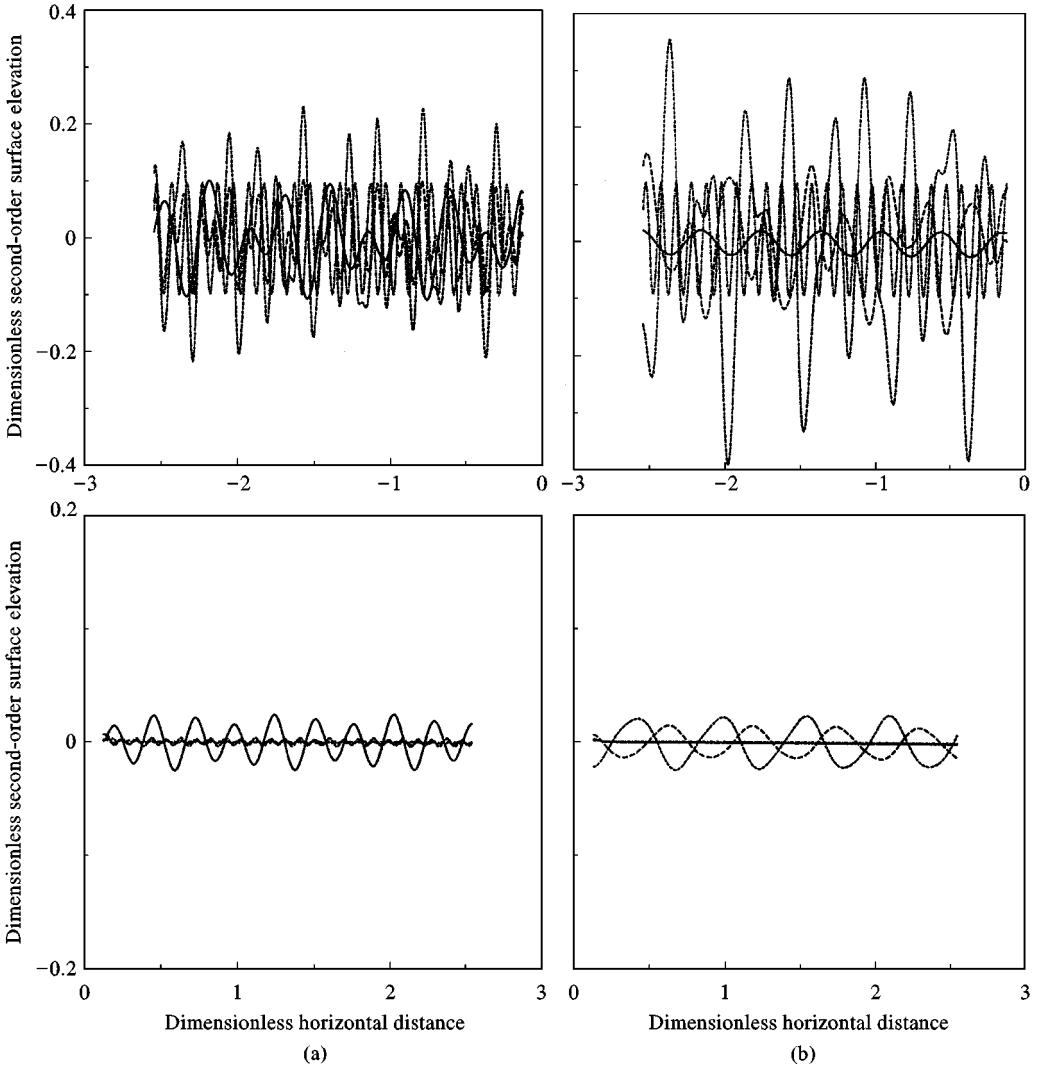

Figure 7. Second-order (a) sum-frequency and (b) difference-frequency surface elevation components at time $t = 0$ for $k_1h = 1$, $k_2h = 4$, $b/h = 1$, and $d/h = 0{\cdot}2$. Notation: ———, $(\omega_1 \pm \omega_1)$; –·–·–, $(\omega_2 \pm \omega_2)$ components; – – – – – – –, $(\omega_1 \pm \omega_2)$ components; — — —, $(\omega_2 \pm \omega_1)$ components.

approach (or something similar), is that quantities such as surface elevation may be determined. Figures 7–10 present the free-surface elevation components at time $t = 0$, upwave and downwave of the structure for two different wave conditions. In these figures the spatial ordinate is nondimensionalized by the cylinder draft d and is measured from the origin of the global coordinate system as shown in Figure 1. Negative values of this ordinate denote locations upwave of the structure, while positive values indicate downwave locations. All surface elevations in these figures are nondimensionalized by $(H_1 + H_2)/4$.

Figure 7 presents the dimensionless second-order sum- and difference-frequency surface elevation components for $k_1h = 1$, $k_2h = 4$, $b/h = 1$ and $d/h = 0{\cdot}2$. It can be seen that there is a dramatic reduction in the amplitudes of the second-order wave components downwave

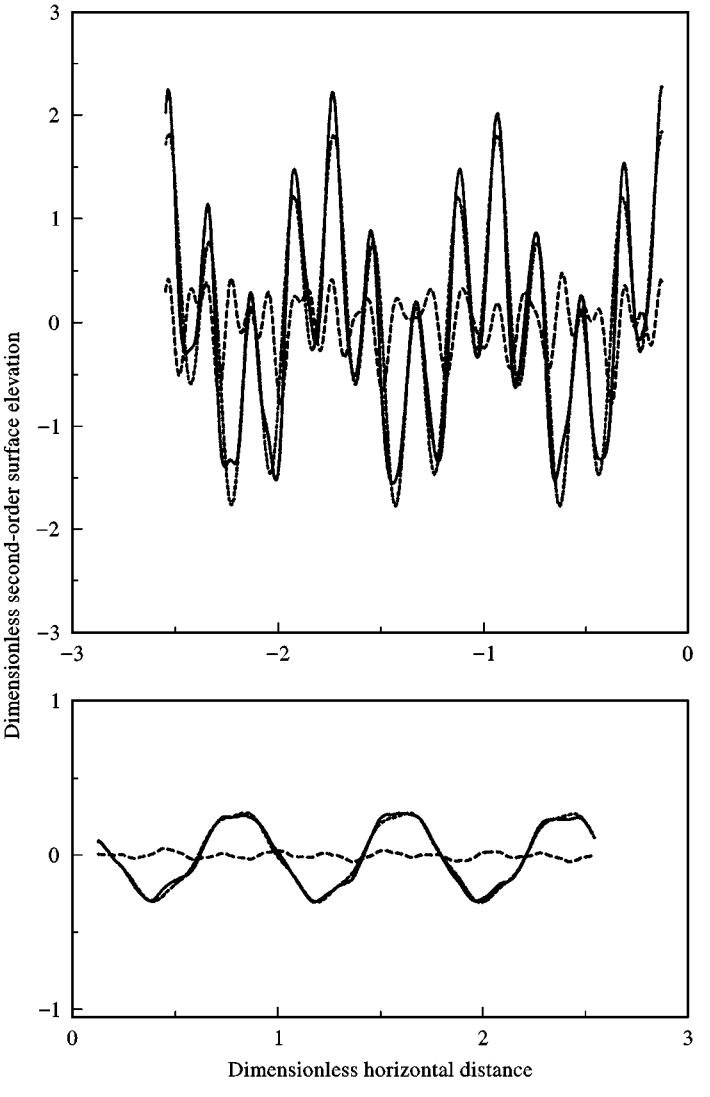

Figure 8. First-order, second-order and total surface elevation components at time $t = 0$ for $k_1h = 1$, $k_2h = 4$, $b/h = 1$, $H_1/h = H_2/h = 0{\cdot}1$, and $d/h = 0{\cdot}2$. Notation:– – – – – –, -first-order components; — — —, second-order components; ———, total (first-plus second-order).

of the structure, and that this decrease occurs for both the sum- and difference-frequency components.

Figure 8 presents the corresponding first-order, second-order and total surface elevations upwave and downwave of the structure at time $t = 0$. The reflected wave field is clearly apparent in the figure; furthermore, it can be seen that even though the second-order wave components may contribute significantly to the total loading on the structure, the transmitted wave field is essentially linear. These results are for an incident wave system in which all components are in phase at $x = 0$. Clearly, the relative phasing of the various wave components may have a significant influence on the numerical results.

Table 1 presents the amplitudes of the first-order, second-order and total free-surface elevations at the upwave and downwave edges of the cylinder (i.e., the wave run-up components) for the same data used to generate Figures 7 and 8. It can be seen that the maxima of the first- and second-order run-up do not occur simultaneously; consequently the maximum total run-up is less than the sum of the first- and second-order components.

Figures 9 and 10 present similar data to Figures 7 and 8, respectively, but for the case $k_1h = 1{\cdot}5$, $k_2h = 3{\cdot}5$. The conclusions regarding the earlier case are also true here, i.e., the structure presents an effective filter to the transmission of the second-order wave field.

Table 2 presents the amplitudes of the first-order, second-order and total wave run-up components at the upwave and downwave edges of the cylinder for the same data used to

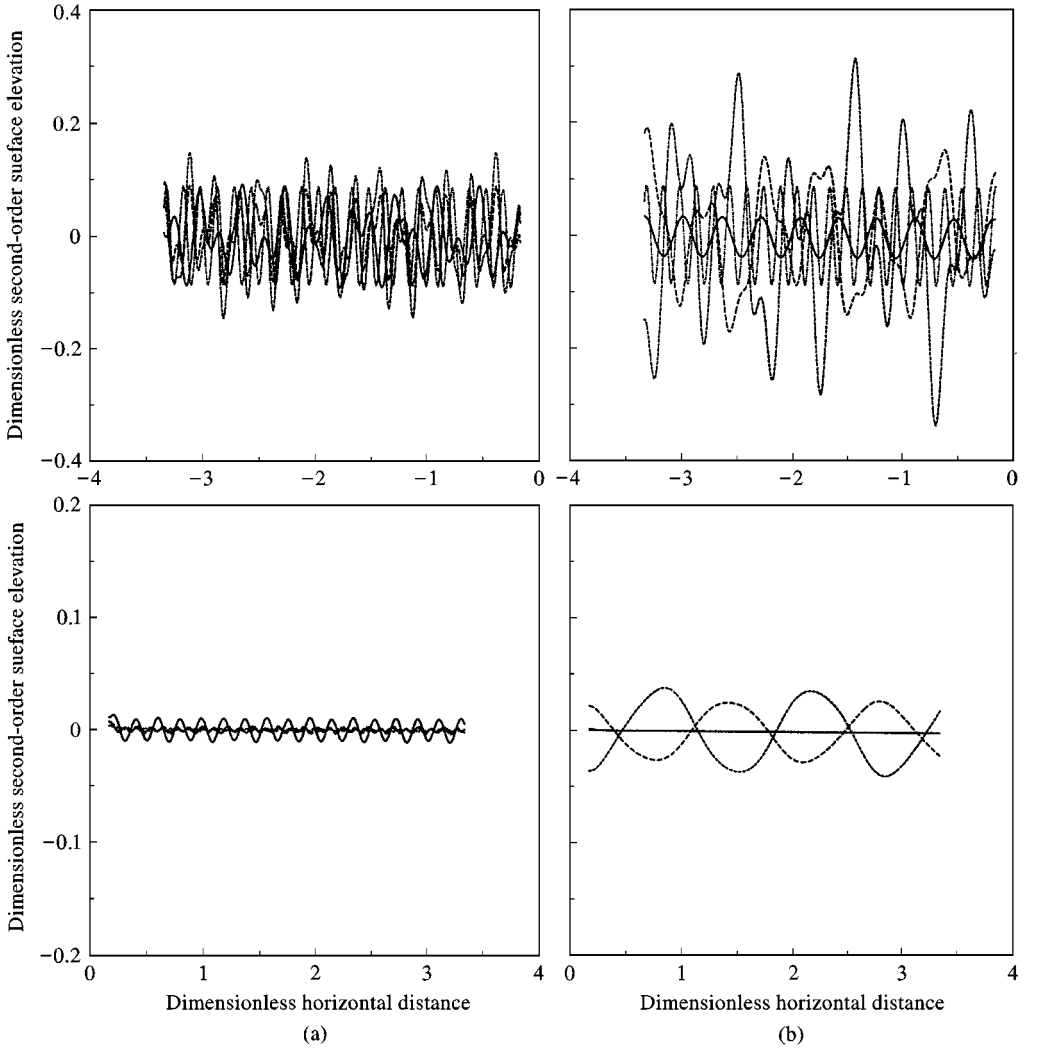

Figure 9. Second-order (a) sum-frequency and (b) difference-frequency surface elevation components at time $t = 0$ for $k_1h = 1{\cdot}5$, $k_2h = 3{\cdot}5$, $b/h = 1$, and $d/h = 0{\cdot}2$. Notation: ———, $(\omega_1 \pm \omega_1)$ components; –·–·–, $(\omega_2 \pm \omega_2)$ components; – – – – – – –, $(\omega_1 \pm \omega_2)$ components; — — —, $(\omega_2 \pm \omega_1)$ components.

TABLE 1

Amplitudes of first-order, second-order and total surface elevations at upwave and downwave edges of cylinder for $k_1h = 1$, $k_2h = 4$, $b/h = 1$, $H_1/h = H_2/h = 0{\cdot}1$, and $d/h = 0{\cdot}2$

	Upwave ($x = -b$)	Downwave ($x = b$)
First-order surface elevation	1·925	0·310
Second-order surface elevation	0·515	0·049
Total surface elevation	2·307	0·324

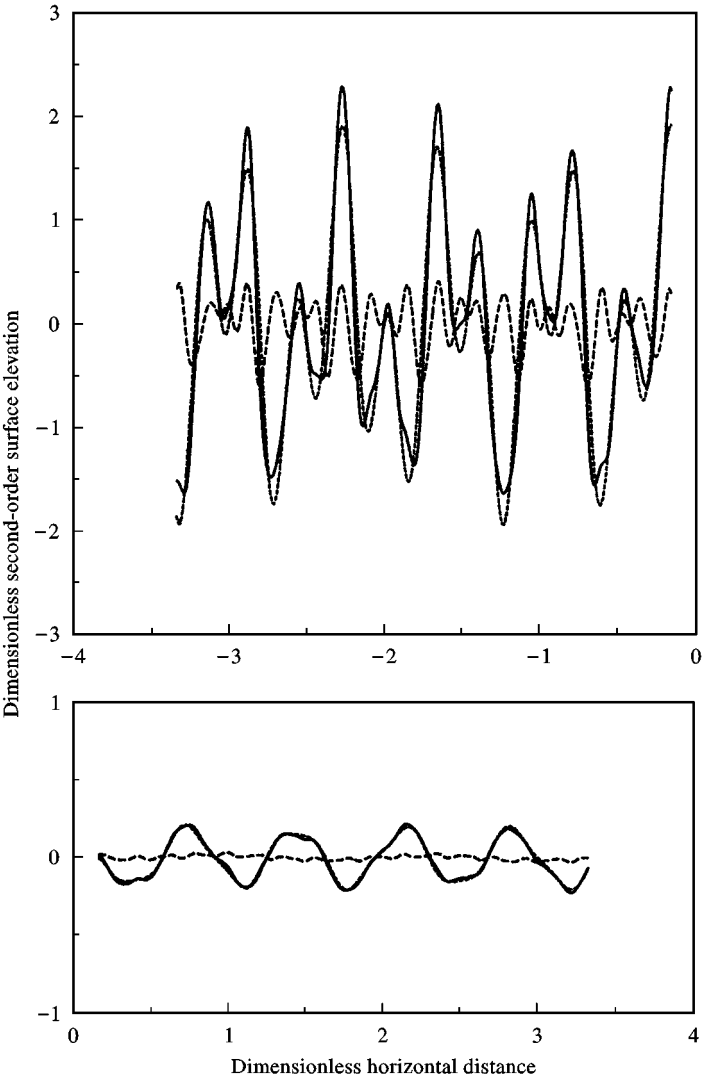

Figure 10. First-order, second-order and total surface elevation components at time $t = 0$ for $k_1h = 1{\cdot}5$, $k_2h = 3{\cdot}5$, $b/h = 1$, $H_1/h = H_2/h = 0{\cdot}1$, and $d/h = 0{\cdot}2$: – – –, first-order components; — — —, second-order components; ———, total (first-plus second-order).

TABLE 2

Amplitudes of first-order, second-order and total surface elevations at upwave and downwave edges of cylinder for $k_1h = 1{\cdot}5$, $k_2h = 3{\cdot}5$, $b/h = 1$, $H_1/h = H_2/h = 0{\cdot}1$, and $d/h = 0{\cdot}2$

	Upwave ($x = -b$)	Downwave ($x = b$)
First-order surface elevation	1·970	0·225
Second-order surface elevation	0·424	0·049
Total surface elevation	2·283	0·236

generate Figures 9 and 10. Again, it can be seen that first- and second-order run-up components are not in phase and the upwave values are significantly larger than the downwave ones.

4. CONCLUSIONS

A complete second-order solution has been presented for the diffraction of bichromatic Stokes waves by a semi-immersed rectangular cylinder. Analytical expressions have been developed for the fluid velocity potentials at both first- and second-order in the three fluid domains; upwave, downwave, and beneath the structure. Numerical results have been presented for the sum- and difference-frequency hydrodynamic loads, and the free-surface elevations upwave and downwave of the structure. For the range of wave amplitudes and frequencies considered herein it is found that although the second-order hydrodynamic loads on the structure may be significant, the transmitted wave field is essentially linear.

ACKNOWLEDGEMENT

This work was supported in part by the Texas Advanced Technology Program (Project No. 003652-856). This support is gratefully acknowledged.

REFERENCES

ISAACSON, M. & CHEUNG, K. F. 1990 Time domain solution for second-order wave diffraction. *ASCE Journal of Waterway, Port, Coastal and Ocean Division* **116,** 191–210·

ISAACSON, M. & CHEUNG, K. F. 1991 Second-order wave diffraction around two-dimensional bodies by time domain method. *Applied Ocean Research* **13,** 175–186.

ISAACSON, M. & NG, J. Y. T. 1993 Time domain second-order wave radiation in two dimensions. *Journal of Ship Research* **37,** 25–33.

LIGHTHILL, M. J. 1979 Waves and hydrodynamic loading. *Proceedings Behavior of Offshore Structures* (BOSS), London, U.K., pp. 1–40.

MIAO, G. P. & LIU, Y. Z. 1986 A theoretical study of the second-order wave forces for two-dimensional bodies. *Proceedings of the 5th International Offshore Mechanics and Arctic Engineering Conference*, Tokyo, Japan, pp. 330–336.

MOLIN, B. 1979 Second-order diffraction loads on three-dimensional bodies. *Applied Ocean Research* **1,** 197–202.

NEWMAN, J. N. 1990 Second-harmonic wave diffraction at large depths. *Journal of Fluid Mechanics* **213,** 59–70.

SARPKAYA, T. & ISAACSON, M. 1981 *Mechanics of Wave Forces on Offshore Structures*. New York: Van Nostrand Reinhold.

SULISZ, W. 1993 Diffraction of second-order surface waves by semi-submerged horizontal rectangular cylinder. *ASCE Journal of Waterway, Port, Coastal and Ocean Division* **119,** 160–171.

SULISZ, W. & JOHANSSON, M. 1992 Second-order wave loading on a horizontal rectangular cylinder of substantial draught. *Applied Ocean Research* **14,** 333–340.
VADA, T. 1987 A numerical solution of the second-order wave diffraction problem for a submerged cylinder of arbitrary shape. *Journal of Fluid Mechanics* **174,** 23–37.
WU, G. X. 1991 On the second-order reflection and transmission by a horizontal cylinder. *Applied Ocean Research* **13,** 58–62.
WU, G. X. 1993a Second-order wave radiation by a submerged horizontal circular cylinder. *Applied Ocean Research* **15,** 293–303,
WU, G. X. 1993b Hydrodynamic forces on a submerged circular cylinder undergoing large-amplitude motion. *Journal of Fluid Mechanics* **254,** 41–58.
WU, G. X. & EATOCK TAYLOR, R. 1990 The second-order diffraction force on a horizontal cylinder. *Applied Ocean Research* **12,** 106–111.